Analytical and numerical approaches to piezoelectric bimorph

Amâncio Fernandes [a], Joël Pouget [b,*]

[a] *Laboratoire de Modélisation en Mécanique (UMR 7607), Université Pierre et Marie Curie, Case 162,
4 Place Jussieu, 75252 Paris Cedex 05, France*
[b] *Laboratoire d'Etudes Mécaniques des Assemblages (FRE 2481), Université de Versailles/Saint-Quentin-en-Yvelines,
Bâtiment Descartes, 45 Ave des Etats-Unis, 78035 Versailles Cedex, France*

Abstract

We propose an efficient and accurate approach to piezoelectric bimorph based on a refined expansion of the elastic displacement and electric potential. The field approximation of the through-the-thickness variation accounts for a shear correction and a layerwise modelling for the electric potential. A particular attention is devoted to the boundary conditions on the bottom and top faces of the plate as well as to the interface continuity conditions for the electromechanical variables. The continuity condition on the electric potential imposes some restrictions on the approximation of the electric potential. Moreover, the continuity condition on the normal component of the electric induction at the bimorph interface is ensured by a Lagrange multiplier. The equations of the piezoelectric bimorph are obtained by using variational formulation involving the appropriate boundary and continuity conditions.

A selection of numerical illustrations is presented for the series and parallel piezoelectric bimorphs simply supported under cylindrical bending conditions. Two types of electromechanical load are considered (i) a surface density of force applied on the top face and (ii) an electric potential applied on the bottom and top faces of the bimorph. The results thus obtained are compared to those provided by finite element computations performed for the full 3D model and by a simplified model without shear effect. At last, the problem of piezoelectric bimorph vibration is also examined for both closed and open circuit conditions. Excellent predictions with low error estimates of the local (profile) and global responses as well as resonant frequencies are observed. The comparisons assess of the effectiveness of the present approach to piezoelectric bimorph.
© 2003 Elsevier Ltd. All rights reserved.

Keywords: Piezoelectric bimorph; Higher order plate theory; Actuators; Vibration control

1. Introduction

The study of novel materials made of composite structures equipped with piezoelectric components remains an active research area and success of *adaptive devices* has attracted the attention of industry and

* Corresponding author. Tel.: +33-1-39-25-42-09; fax: +33-1-39-25-30-15.
E-mail address: joel.pouget@meca.uvsq.fr (J. Pouget).

engineering researchers due to numerous technological applications (see for review Rao and Sunar, 1994; Tani et al., 1998; Chee et al., 1998). The analysis of *piezoelectric composites* such as laminated plates requires modelling with efficiently accurate approximation of both *sensor* and *actuator* functions. One of the most popular advantage of piezoelectric material is when an electric potential is applied to a piezoelectric component its dimensions change. Conversely, when it is stressed mechanically by a force, it generates electric charges on its faces. If the electrodes are not short-circuited an electric current associated with the electric charges can be measured. The most popular simple piezoelectric actuator consists usually of a slab of piezoelectric ceramics when an electric field is placed across its thickness, the layer expands or contracts mainly in its length direction. However, the motion of a single layer is extremely small (the order of fewer micrometer for a voltage of 100 V). To overcome this limitation, piezoelectric composites using *flexural–extensional deformation* becomes necessary. One of the most practical multilayer piezoelectric composites commonly used is the *piezoelectric bimorph* or *bender*. The application of an electric field across the two layers of the bender produces one layer to expand while the other one contracts. The global result is thus a flexural deformation much greater than the length or thickness deformation of the individual layers (of the order of few hundreds of micrometers for 100 V). More sophisticated multiplayer piezoelectric composites could be considered to improve the motion amplification and performance of the adaptive structure (Steel et al., 1978). Wide range of interesting technological applications have been proposed, going from aeronautical and automotive structures (shape control of space antennas, active or passive control of vibrations, etc.) to many other engineering devices (see Lee, 1979; Muralt et al., 1986; Peters and Blackford, 1989; Chonan et al., 1996; Yoon and Washington, 1998; for quoted examples).

The main objective of the present study attempts to present a consistent and efficient approach to piezoelectric bimorph structure. Although a number of consistent and efficient approaches to piezoelectric bimorph have been proposed by Spineau et al. (1998), He et al. (2000) and Lim et al. (2001), most of these models are mostly based on the kinematic assumption of Love–Kirchhoff theory of thin elastic plates or Bernoulli–Euler theory of beams as proposed by Smits et al. (1991a), Smits and Cooney (1991b) and Crawley and Anderson (1990). These models are able to accurately predict the global responses of the bimorph, especially the deflection, but they cannot provide excellent estimates of the local responses such as the through-the-thickness variations of the displacements, electric potential and stresses. The classification of the various approaches is mainly based on the kinematic assumption for approximating the through-the-thickness variation of the electromechanical state variables and representation method of the piezoelectric layers (see Saravanos and Heyliger, 1999; for a review). Here, we propose an alternative approach based on a combination of mixed through-the-thickness approximation including shear correction for the elastic displacement. More precisely, the present modelling combines an equivalent single-layer representation for the mechanical displacement with a layerwise-type approximation for the electric potential. Moreover, the modelling, presented hereafter, accounts for the conservation law of electric charge (Gauss equation). We do not therefore consider any hypothesis on the form of the electric induction.

The plate equations are derived from a variational formulation extended to piezoelectric media. A particular attention is devoded to the continuity conditions at the layer interface and to the boundary conditions on the top and bottom faces of the plate. The present study is a continuation of work mostly dedicated to single layer plate model where all the requisite ingredients have been discussed in detail by Fernandes and Pouget (2001). Extension of the later approach to multilayer plate has been proposed leading to particularly interesting comparisons to finite element computation for different kinds of electromechanical loads has been proposed by Fernandes and Pouget (2002). In order to assess the capability and performance of the model, a number of benchmark tests are given for a piezoelectric bimorph subject to (i) a force density normal to the upper face and (ii) an electric potential applied to the bottom and top faces of the plate and eventually at the layer interface. Some comparisons to numerical results provided by finite element method performed on the fully 3D model are considered. The comparisons lead to very excellent predictions of both global (displacement, electric charge) and local (thickness variations of the

electromechanical state) responses of the piezoelectric bimorph. The vibration of the piezoelectric structure is then examined for the shorted and open circuit providing also very accurate results.

The outline of the study is organized as follows: the piezoelectricity formulation is briefly stated in Section 2. The approximation of the electromechanical fields is given in Section 3, the approach is then specialized according to the bimorph arrangement. A particular emphasis is placed, in Section 4, on the boundary and interface conditions for the series and parallel configurations. In Section 5, the bimorph equations are then derived from the variational formulation along with the associated mechanical and electric boundary conditions around the plate contour. The study of the piezoelectric bimorph under cylindrical bending is examined in Section 6 and numerical results and comparisons to finite element computations are also given. Section 7 is devoted to vibration modes of the piezoelectric bimorph and comparisons to finite element method are also presented. At last the closing remarks and discussion of the most relevant results are evoked in Section 8.

2. Piezoelectricity formulation: pre-requisites

In this section, we summarize the ingredients concerning piezoelectricity needed for the present plate approach. The formulation is based on *Hamilton's principle* extended to piezoelectricity (see Tiersten, 1969). The variational principle can be stated as

$$\delta \int_{t_1}^{t_2} \int_{\Omega} \mathscr{L} \, \mathrm{d}v \, \mathrm{d}t + \int_{t_1}^{t_2} \delta W \, \mathrm{d}t = 0, \tag{1}$$

where $\mathscr{L} = K - H(S_{ij}, E_i)$ is the density of the *Lagrangian functional* with K, the *kinetic energy* $K = \frac{1}{2}\rho \dot{u}_i \dot{u}_i$ and H, the *electric enthalpy density function*. In addition, ρ is the mass density, u_i the elastic displacement (the dot means derivative with respect to time). The enthalpy density function for piezoelectricity takes on the form

$$H(S_{ij}, E_i) = \frac{1}{2}\sigma_{ij}S_{ij} - \frac{1}{2}D_i E_i, \tag{2}$$

where $S_{ij} = \frac{1}{2}(u_{i,j} + u_{j,i})$ is the strain tensor component, E_i is the electric field vector, σ_{ij} are the components of the stress tensor and D_i represents the electric displacement or induction vector. The last term in Eq. (1) is the virtual work of the prescribed mechanical and electric quantities on the domain boundary $\partial\Omega$ given by

$$\delta W = \int_{\partial\Omega} T_i \, \delta u_i \, \mathrm{d}s + \int_{\partial\Omega} Q \, \delta\phi \, \mathrm{d}s. \tag{3}$$

In Eq. (3), **T** is the surface traction and Q is the surface density of electric charge applied to the domain boundary $\partial\Omega$. The scalar variable ϕ is the electric potential. In addition, in the framework of the *quasi-electrostatic approximation*, the electric field derives from an electric potential $E_i = -\phi_{,i}$. On using a classical argument of integration by part and assuming arbitrary variations δu_i and $\delta\phi$ throughout the domain Ω subject to the conditions $\delta\phi(t_1) = \delta\phi(t_2) = 0$ and $\delta u_i(t_1) = \delta u_i(t_2) = 0$. The field equations (in absence of body force) are

$$\sigma_{ij,j} = \rho\ddot{u}_i, \quad D_{i,i} = 0. \tag{4}$$

The above field equations are completed by boundary conditions for the prescribed surface traction and surface density of electric charge or electric potential, namely $\sigma_{ij}n_j = T_i$ on $\partial\Omega_\sigma$, $u_i = \bar{u}_i$ on $\partial\Omega_u$ and $D_i n_i = Q$ on $\partial\Omega_D$, $\phi = \bar{\phi}$ on $\partial\Omega_\phi$ ($\partial\Omega = \partial\Omega_\sigma \cup \partial\Omega_u$ and $\partial\Omega = \partial\Omega_D \cup \partial\Omega_\phi$ with $\partial\Omega_\sigma \cap \partial\Omega_u = \partial\Omega_D \cap \partial\Omega_\phi = \phi$). For linear piezoelectricity the enthalpy density function usually has the form (see Ikeda, 1996)

$$H(S_{ij}, E_i) = \frac{1}{2}C_{ijpq}^{\mathrm{E}} S_{ij} S_{pq} - e_{ipq} E_i S_{pq} - \frac{1}{2}\varepsilon_{ij}^{\mathrm{S}} E_i E_j. \tag{5}$$

It has been assumed isothermal process and thermomechanical coupling and pyroelectric effects have been neglected. The constitutive equations for σ and $\mathbf{D}$ derive from the enthalpy functional as follows

$$\begin{cases} \sigma_{ij} = \dfrac{\partial H}{\partial S_{ij}} = C^{E}_{ijpq}S_{pq} - e_{kij}E_k, \\ D_i = -\dfrac{\partial H}{\partial E_i} = e_{ipq}S_{pq} + \varepsilon^{S}_{ij}E_j. \end{cases} \tag{6}$$

In Eq. (6), $\mathbf{C}^{E}$ is the fourth-order tensor of elasticity coefficients measured at a constant electric field, $\mathbf{e}$ is the third-order tensor of piezoelectric coefficients and ε^{S} is the second-order tensor of the dielectric coefficients measured at a constant strain. According to the material symmetry the number of independent constants can be reduced. In the case of isotropically transverse symmetry we have five elastic coefficients, three piezoelectric constants and two dielectric constants which are independent (examples of piezoelectric materials are given in Ikeda (1996) and Cady (1964)).

3. Field approximation

Along with the accepted kinematic assumptions for the displacement field in most plate theories (e.g. Reddy, 1984), we consider an expansion of the elastic displacement as a series function of the thickness coordinate. The level of truncation of the expansion leads to the order of the plate theory (Bisegna and Caruso, 2001). In the framework of the present approach, the elastic displacement and electric potential are assumed to be of the form

$$\begin{cases} u_\alpha(x,y,z,t) = U_\alpha(x,y,t) - zw_{,\alpha}(x,y,t) + f(z)\gamma_\alpha(x,y,t), \quad \alpha \in \{1,2\}, \\ u_3(x,y,z,t) = w(x,y,t), \\ \phi^{(\ell)}(x,y,z,t) = \phi_0^{(\ell)}(x,y,t) + z_\ell\phi_1^{(\ell)}(x,y,t) + P_\ell(z_\ell)\phi_2^{(\ell)}(x,y,t) + g(z)\phi_3^{(\ell)}(x,y,t), \end{cases} \tag{7}$$

with $\ell = 1$ for the lower layer and $\ell = 2$ for the upper layer in the case of bimorph structure (the notations of the geometry and coordinates are given in Fig. 1). We have set $z_1 = z + h/4$ and $z_2 = z - h/4$ the local thickness coordinates attached to the lower and upper layers, respectively. It is worthwhile commenting the expressions (7): (i) In Eq. (7)$_1$, U_α holds for the *middle plane displacement component*, w is the *deflection* and γ_α represents the *shear function*. All the functions are defined at the middle plane coordinate $(x,y,0)$. (ii) If $f(z) = 0$, we recover the classical Kirchhoff–Love thin plate theory (Love, 1944), if $f(z) = z$ we obtain the Mindlin–Reissner model or the first-order theory (Reissner, 1975). The expansion of $f(z)$ at higher-order leads to a refined model as developed by Reddy (1984). (iii) In the present modelling, we propose the following functions
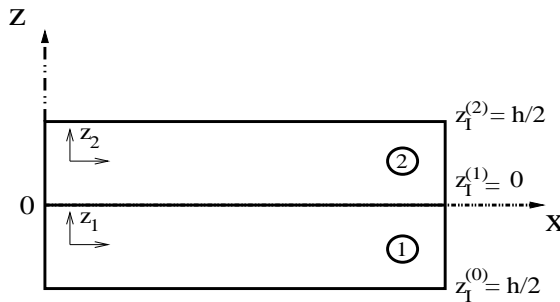

Fig. 1. Piezoelectric bimorph: coordinates and geometry.

$$\begin{cases} P_1(z) = z(z+h/2), \quad P_2(z) = z(z-h/2), \\ f(z) = \dfrac{h}{\pi}\sin\left(\dfrac{\pi z}{h}\right), \quad g(z) = \dfrac{h}{\pi}\cos\left(\dfrac{\pi z}{h}\right), \end{cases} \tag{8}$$

where h is the plate thickness which is supposed to be uniform. The case of purely elastic plates has been extensively studied by Touratier (1991) with extension to elastic shells (Touratier, 1992). (iv) For the electric potential, the first two terms are associated with the applied electric potential on the plate faces since $P_1(-h/2) = 0$, $P_2(h/2) = 0$ and $g(\pm h/2) = 0$. The third terms is referred as to the *induced electric potential* by piezoelectric coupling in the upper or lower layer. The term factor of $g(z)$ is associated with the shearing effect.

4. Boundary and continuity conditions

Two piezoelectric bimorph arrangements are commonly considered and manufactured. The first kind of bimorph shown in Fig. 2(a) is often called *series bimorph* or *antiparallel bimorph*. In this situation both piezoelectric layers are made of identical materials and have the same thickness 0.5h, however, the piezo-active axes are in opposite direction. The electric potential is applied to the bottom and top faces through thin metallic electrodes. The second arrangement is known as *parallel piezoelectric bimorph* and it has an intermediate electrode at the layer interface as depicted in Fig. 2(b). In this case the piezo-active axes are in the same direction. For both arrangements the electric field along the thickness coordinate across each layer is of the order of $2V/h$.

4.1. Series or antiparallel piezoelectric bimorph

Now, we must consider the boundary and continuity conditions along with the symmetry properties of the bimorph. The boundary conditions on the electric potential on the plate faces can be written as

$$\begin{cases} \phi^{(1)}(x,y,-h/2) = \phi_0^{(1)} - \dfrac{h}{4}\phi_1^{(1)} = -V, \\ \phi^{(2)}(x,y,+h/2) = \phi_0^{(2)} + \dfrac{h}{4}\phi_1^{(2)} = V. \end{cases} \tag{9}$$

The continuity condition at the bimorph interface $z = 0$ can be expressed as

$$\begin{cases} \phi^{(1)}(x,y,0) = \phi^{(2)}(x,y,0), \\ D_3^{(1)}(x,y,0) = D_3^{(2)}(x,y,0). \end{cases} \tag{10}$$

For the electric potential we use the expansion (7)₃

$$\phi_0^{(1)} + \frac{h}{4}\phi_1^{(1)} + \frac{\pi}{h}\phi_3^{(1)} = \phi_0^{(2)} - \frac{h}{4}\phi_1^{(2)} + \frac{\pi}{h}\phi_3^{(2)}. \tag{11}$$
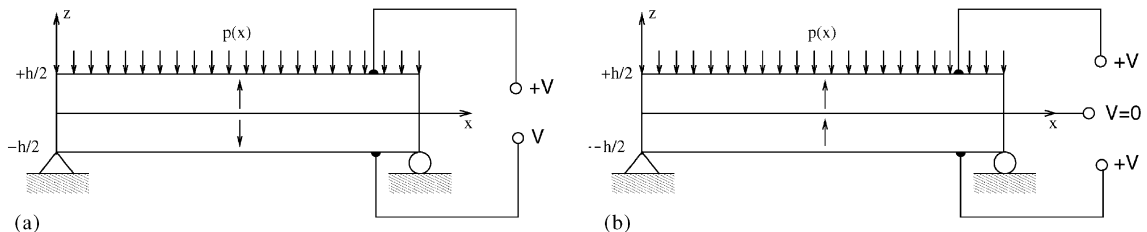

Fig. 2. Piezoelectric bimorph: (a) series arrangement and (b) parallel arrangement.

The continuity condition on the normal electric induction component can be written by using the constitutive equation (6). Moreover, piezoelectric layers are made of identical *transversaly isotropic material* but having their piezoelectric axis in opposite direction along the *z*-axis. Then we have $D_3^{(\ell)} = e_{3\alpha\beta}^{*(\ell)} S_{\alpha\beta} + \varepsilon_{33}^{*(\ell)} \phi_{,3}^{(\ell)}$ with $\ell \in \{1, 2\}$. The symmetry conditions leads to $e_{3\alpha\beta}^{*(2)} = -e_{3\alpha\beta}^{*(1)} = e_{3\alpha\beta}^*$ ($\alpha, \beta \in \{1, 2\}$) and $\varepsilon_{33}^{*(1)} = \varepsilon_{33}^{*(2)} = \varepsilon_{33}$. Where the effective piezoelectric constant $e_{3\alpha\beta}^*$ and dielectric constants ε_{33}^* are derived from the hypothesis on the normal shear stress σ_{33} (σ_{33} negligible, see Appendix A for the definitions of the effective material constants). Finally, the continuity condition on D_3 takes on the form

$$-e_{3\alpha\beta}^* S_{\alpha\beta}^{(0)} - \varepsilon_{33}^* \left(\phi_1^{(1)} - \frac{h}{2} \phi_2^{(1)} \right) = e_{3\alpha\beta}^* S_{\alpha\beta}^{(0)} - \varepsilon_{33}^* \left(\phi_1^{(2)} + \frac{h}{2} \phi_2^{(2)} \right),$$

or

$$-2e_{3\alpha\beta}^* S_{\alpha\beta}^{(0)} = \varepsilon_{33}^* \left(\phi_1^{(1)} - \phi_1^{(2)} \right) - \frac{h}{2} \varepsilon_{33}^* \left(\phi_2^{(1)} + \phi_2^{(2)} \right). \tag{12}$$

where $S_{\alpha\beta}^{(0)} = U_{(\alpha,\beta)}$. The solution $\phi_0^{(2)} = -\phi_0^{(1)} = V/2$, $\phi_1^{(1)} = \phi_1^{(2)} = (2/h)V$ and $\phi_3^{(1)} = \phi_3^{(2)}$ satisfies the conditions given by Eqs. (9) and (11). The condition (12) reduces to (with indice summation on α and β)

$$A_\theta = \phi_2^{(1)} + \phi_2^{(2)} - \frac{4}{h} \frac{e_{3\alpha\beta}^*}{\varepsilon_{33}^*} S_{\alpha\beta}^{(0)} = 0. \tag{13}$$

The above equation tells us that if there is no global elongational motion of the bimorph, therefore $\phi_2^{(1)} + \phi_2^{(2)} = 0$, which occurs for a pure flexural motion. At last, the form of the electric potential is

$$\phi^{(\ell)} = 2\frac{V}{h}z + P_\ell(z)\phi_2^{(\ell)} + g(z)\phi_3, \tag{14}$$

with $\ell \in \{1, 2\}$. With the view of solving the piezoelectric bimorph problem we must find the nine unknown functions $\{U_\alpha, w, \gamma_\alpha, \phi_2^{(1)}, \phi_2^{(2)}, \phi_3, \theta\}$ with $\alpha \in \{1, 2\}$ and θ being the Lagrange multiplier. The problem can be now stated as follows, find the nine unknown functions under the constraint (13) relating $\phi_2^{(\ell)}$ to U_α.

4.2. Parallel piezoelectric bimorph

For this arrangement, a zero voltage ($V = 0$) is applied to the intermediate electrode, while the voltage V is applied to the bottom and top faces of the plate. In such a situation, the components of the electric field along the thickness direction E_3 across the lower and upper layers are in opposite directions. Accordingly, regarding to the piezoelectric couplings, this case is, in fact, similar to the antiparallel situation. The boundary and interface conditions on the electric potential are the following

$$\begin{cases} \phi^{(1)}(x, y, -h/2) = \phi_0^{(1)} - \frac{h}{4}\phi_1^{(1)} = V, \\ \phi^{(1)}(x, y, 0) = \phi_0^{(1)} + \frac{h}{4}\phi_1^{(1)} + \frac{h}{\pi}\phi_3^{(1)} = 0, \\ \phi^{(2)}(x, y, 0) = \phi_0^{(2)} - \frac{h}{4}\phi_1^{(2)} + \frac{h}{\pi}\phi_3^{(2)} = 0, \\ \phi^{(2)}(x, y, +h/2) = \phi_0^{(2)} + \frac{h}{4}\phi_1^{(2)} = V. \end{cases} \tag{15}$$

The continuity condition at the bimorph interface on the electric potential is fulfilled. On using symmetry argument on the electric potential, it can be shown $\phi_0^{(1)} = \phi_0^{(2)} = \phi_0$, $\phi_1^{(1)} = -\phi_1^{(2)} = \phi_1$, and $\phi_3^{(1)} = \phi_3^{(2)} =$

ϕ_3. It is worthwhile noting, in this situation, there is no continuity condition on the normal component of the electric induction. The electric potential for both layers takes on the form

$$\begin{cases} \phi^{(1)} = \dfrac{1}{2}\left(1 - 4\dfrac{z}{h}\right)V + P_1(z)\phi_2^{(1)} + \hat{g}_1(z)\phi_3, \\ \phi^{(2)} = \dfrac{1}{2}\left(1 + 4\dfrac{z}{h}\right)V + P_2(z)\phi_2^{(2)} + \hat{g}_2(z)\phi_3, \end{cases} \tag{16}$$

where we have set

$$\hat{g}_1(z) = \frac{h}{\pi}\left[\frac{\pi}{h}g(z) - 1 - 2\frac{z}{h}\right] \quad \text{and} \quad \hat{g}_2(z) = \frac{h}{\pi}\left[\frac{\pi}{h}g(z) - 1 + 2\frac{z}{h}\right].$$

Now, the problem amount to finding the eight unknown functions $\{U_\alpha, w, \gamma_\alpha, \phi_2^{(1)}, \phi_2^{(2)}, \phi_3\}$ with $\alpha \in \{1, 2\}$. However, in the present situation there is no condition on the electric induction as in the series bimorph.

Remark. Surface density of electric charge can be applied on the top and bottom faces of the bimorph. In this situation, the boundary condition on the electric induction is reduced to $D_3(x, y, \pm h/2) = Q(x, y)$, where Q is the prescribed electric charge per unit of area (see for details Fernandes and Pouget, 2001). The continuity of the electric potential and normal component of the electric induction must be satisfied, thereby, there is no difference between the series and parallel arrangements except if the intermediate electrode is at the ground for the parallel bimorph (no continuity condition on D_3).

5. Equations of motion for the bimorph structure

The variational formulation stated in Section 2 is then used to derive the equations of motion of the two-dimensional model from the full three-dimensional formulation of piezoelectricity. The expansion of the elastic displacement and electric potential equations (7) and (14) or (16) according to the arrangement are substituted into the formulation (1) and the dependency of the field on the thickness coordinate z is rubbed out by integrating over the plate thickness. The variational formulation must be written under the constraint (13) involving the introduction of a Lagrange multipliers θ. At last the Hamiltonian principle can be cast into the form (see for details Fernandes and Pouget, 2002)

$$\int_{t_1}^{t_2} (\delta K - \delta U + \delta W_1 + \delta W_2 + \delta \Lambda)\,\mathrm{d}t = 0. \tag{17}$$

In Eq. (17) the first term represents the variation of the kinetic energy given by

$$\delta K = -\int_\Sigma \left(\Gamma_\alpha^{(u)}\,\delta U_\alpha + \Gamma^{(w)}\,\delta w + \Gamma_\alpha^{(\gamma)}\,\delta\gamma_\alpha\right)\mathrm{d}s - \int_{\mathscr{C}} \widehat{\Gamma}_\alpha^{(w)} n_\alpha\,\delta w\,\mathrm{d}\ell. \tag{18}$$

The different acceleration quantities are defined by

$$\begin{cases} \Gamma_\alpha^{(u)} = I_0\ddot{U}_\alpha, \\ \Gamma^{(w)} = I_0\ddot{w} + I_1\ddot{\gamma}_{\alpha,\alpha} - I_2\ddot{w}_{,\alpha\alpha}, \\ \Gamma_\alpha^{(\gamma)} = I_3\ddot{\gamma}_\alpha - I_2\ddot{w}_{,\alpha}, \\ \widehat{\Gamma}^{(w)} = I_1\ddot{w}_{,\alpha} - I_2\ddot{\gamma}_\alpha, \end{cases} \tag{19}$$

where the different inertial momenta are given by

$$(I_0, I_1, I_2, I_3) = \int_{-h/2}^{+h/2} \rho(1, z^2, f^2(z), zf(z))\,\mathrm{d}z. \tag{20}$$

In Eq. (18), $\mathbf{n}$ is the outwards unit normal to the plate contour $\mathscr{C}$. The second term in Eq. (17) is the variation of the internal force work

$$\delta U = \int_{\Sigma} \left\{ N_{\alpha\beta}(\delta U_{\alpha})_{,\beta} - M_{\alpha\beta}(\delta w)_{,\alpha\beta} + \widehat{M}_{\alpha\beta}(\delta\gamma_{\alpha})_{,\beta} + \widehat{Q}_{\alpha}\delta\gamma_{\alpha} + D_{\alpha}^{(2)(1)}\delta\phi_{2,\alpha}^{(1)} + D_{\alpha}^{(2)(2)}\delta\phi_{2,\alpha}^{(2)} + D_{\alpha}^{(3)}\delta\phi_{3,\alpha} \right.$$
$$\left. + D_{3}^{(2)(1)}\delta\phi_{2}^{(1)} + D_{3}^{(2)(2)}\delta\phi_{2}^{(2)} + D_{3}^{(3)}\delta\phi_{3} \right\}dS, \tag{21}$$

where the stress and electric charge resultants are computed using the three dimensional stresses σ_{ij} and electric displacement D_i

$$\left(N_{\alpha\beta}, M_{\alpha\beta}, \widehat{M}_{\alpha\beta} \right) = \int_{-h/2}^{+h/2} (1, z, f(z))\sigma_{\alpha\beta}\,dz, \tag{22}$$

$$\widehat{Q}_{\alpha} = \int_{-h/2}^{+h/2} f'(z)\sigma_{\alpha 3}\,dz, \tag{23}$$

$$\left(D_{\alpha}^{(2)(\ell)}, D_{3}^{(2)(\ell)} \right) = \int_{z_{I}^{(\ell-1)}}^{z_{I}^{(\ell)}} \left(P_{\ell}(z)D_{\alpha}^{(\ell)}, P_{\ell}'(z)D_{3}^{(\ell)} \right)dz, \tag{24}$$

$$\left(D_{\alpha}^{(3)}, D_{3}^{(3)} \right) = \sum_{\ell=1}^{2} \int_{z_{I}^{(\ell-1)}}^{z_{I}^{(\ell)}} \left(\hat{g}_{\ell}(z)D_{\alpha}^{(\ell)}, \hat{g}_{\ell}'(z)D_{3}^{(\ell)} \right)dz, \tag{25}$$

with $P'(z) = dP(z)/dz$, $f'(z) = df(z)/dz$ and $g'(z) = dg(z)/dz$.

Remark. There is no fundamental difference between the equation of motion for the series and parallel bimorph since the independent electric potential variation $\{\delta\phi_{2}^{(\ell)}, \delta\phi_{3}\}$ (see Eqs. (14) and (16)) are the same. Nevertheless, the difference between both approximations for the electric potential appears in the definition of the electric charge resultants $D_{\alpha}^{(3)}$ and $D_{3}^{(3)}$, in fact $\hat{g}_{\ell}(z)$ must be replaced by $g(z)$ in Eqs. (24) and (25). The corresponding constitutive equations are then modified.

The third and fourth terms in the variational formulation (17) hold for the variational works of applied forces and electric charges on the faces and lateral contour of the plate. This variational work is the sum of works of prescribed loads on the top and bottom faces of the plate and those on the lateral boundary of the plate, namely

$$\delta W_{1} = \int_{\Sigma} \left(f_{\alpha}\delta U_{\alpha} - p\delta w + \hat{m}_{\alpha}\delta\gamma_{\alpha} + q_{2}^{(1)}\delta\phi_{2}^{(1)} + q_{2}^{(2)}\delta\phi_{2}^{(2)} + q_{3}\delta\phi_{3} \right)dS, \tag{26}$$

$$\delta W_{2} = \int_{\mathscr{C}} \left[F_{\alpha}\delta U_{\alpha} + T\delta w + C_{\alpha}\delta\gamma_{\alpha} - M_{f}(\delta w)_{,n} + Q_{2}^{(1)}\delta\phi_{2}^{(1)} + Q_{2}^{(2)}\delta\phi_{2}^{(2)} + Q_{3}\delta\phi_{3} \right]d\ell - \sum_{p} Z_{p}\delta w_{p}. \tag{27}$$

In Eq. (26), f_{α} and p are surface densities of force, $\hat{m}_{\alpha}$ is a surface moment density. The generalized surface density of electric charges $q_{2}^{(\ell)}$ and q_{3} are zero due to $\hat{g}_{\ell}(\pm h/2) = 0$, and $P_{1}(-h/2) = P_{2}(+h/2) = 0$ (Fernandes and Pouget, 2002).

In Eq. (27), F_{α} and T are densities of force per unit of length, M_{f} and C_{α} are lineic moment densities and Z_{p} are transverse forces applied at angular points of the boundary contour $\mathscr{C}$ of the plate. In Eq. (27), $(\delta w)_{,n}$ is the derivative of the variation δw with respect to the normal direction to the boundary contour. The

electric charges per unit of length $Q_m^{(\ell)}$ are supposed to be zero (the lateral boundary of the plate is not coated with metallic electrode).

Finally the last term in Eq. (17) is the virtual work of force due to the Lagrangian multiplier associated with the constraint (13) and it reads as (Fernandes and Pouget, 2002)

$$\delta \Lambda = \int_{\Sigma} \delta(\theta A_\theta) \, \mathrm{d}S. \tag{28}$$

On accounting for Eq. (13) the virtual work equation (28) can be written as

$$\delta \Lambda = \int_{\Sigma} \left\{ A_\theta \, \delta\theta + \theta \left[-2e_{3\alpha\beta}^* \delta U_{\alpha,\beta} + \frac{h}{2} \varepsilon_{33}^* \left(\delta\phi_2^{(2)} + \delta\phi_2^{(1)} \right) \right] \right\} \mathrm{d}S, \tag{29}$$

Now, by employing integration by part if needed and collecting all the factor of the arbitrary variations $\{\delta U_\alpha, \delta w, \delta\gamma_\alpha, \delta\phi_2^{(\ell)}, \delta\phi_3, \delta\theta\}$ with $\ell \in \{1, 2\}$ to be zero at t_1 and t_2, we arrive at the field equations for the piezoelectric bimorph

$$\begin{cases} \mathcal{N}_{\alpha\beta,\beta} + f_\alpha = \Gamma_\alpha^{(u)}, \\ M_{\alpha\beta,\alpha\beta} - p = \Gamma^{(w)}, \\ \widehat{M}_{\alpha\beta,\beta} - \widehat{Q}_\alpha + \hat{m}_\alpha = \Gamma_\alpha^{(\gamma)}, \\ D_{\alpha,\alpha}^{(2)(\ell)} - \mathscr{D}_3^{(2)(\ell)} = 0, \\ D_{\alpha,\alpha}^{(3)} - D_3^{(3)} = 0, \end{cases} \tag{30}$$

where we have introduced the modified in-plane force resultant and electric induction resultant

$$\begin{cases} \mathcal{N}_{\alpha\beta} = N_{\alpha\beta} - 2e_{3\alpha\beta}^*\theta, \\ \mathscr{D}_3^{(2)(\ell)} = D_3^{(2)(\ell)} + \frac{h}{2} \varepsilon_{33}^*\theta. \end{cases} \tag{31}$$

At last the variation of the Lagrange multiplier θ gives rise to the continuity condition (13) (i.e. $A_\theta = 0$). The associated boundary conditions along the plate contour $\mathscr{C}$ are also deduced from the variational principle equation (17)

$$\begin{cases} F_\alpha = \mathcal{N}_{\alpha\beta} n_\beta & \text{or } U_\alpha \text{ given,} \\ T = \left(\tau_\alpha M_{\alpha\beta} n_\beta \right)_{,s} + n_\alpha M_{\alpha\beta,\beta} + \widehat{\Gamma}_\alpha^{(w)} n_\alpha & \text{or } w \text{ given,} \\ M_f = n_\alpha M_{\alpha\beta} n_\beta & \text{or } w_{,n} \text{ given,} \\ C_\alpha = \widehat{M}_{\alpha\beta} n_\beta & \text{or } \gamma_\alpha \text{ given,} \\ D_\alpha^{(2)(\ell)} n_\alpha = 0 & \text{or } \phi_2^{(\ell)} \text{ given,} \\ D_\alpha^{(3)} n_\alpha = 0 & \text{or } \phi_3 \text{ given,} \end{cases} \tag{32}$$

where s is the curvilinear coordinate along the plate contour $\mathscr{C}$.

Moreover, we have $[\![\tau_\alpha M_{\alpha\beta} n_\beta]\!]_{A_p} = Z_p$ at the angular points A_p of the contour where τ is the tangent vector to the contour $\mathscr{C}$.

It is worthwhile noting that the equations of motion thus obtained is a particular case of more complete equations for piezoelectric plate made of arbitrary layers presented by the authors Fernandes and Pouget (2002). The first two equations (30) are similar to those of the Love–Kirchhoff theory of elastic thin plates, the third equation governs the shearing effects. The last two equations are deduced from the conservation law of electric charges for the generalized electric induction resultants often absent in most theories. It should be noticed that the Lagrange multiplier θ has the dimension of an electric field. It plays the role of an electric field to enforce the continuity of the normal electric induction component at the interface $z = 0$. In the case of the parallel arrangement there is no Lagrange multiplier and we set $\theta = 0$ in Eq. (31).

The *constitutive equations* for the stress and electric charge resultants can be written down as function of the plate deformation and generalized electric potentials $\{U_\alpha, w, \gamma_\alpha, \phi_2^{(\ell)}, \phi_3\}$ and Lagrange multiplier θ by using Eqs. (22)–(25). We substitute the results thus obtained into the plate equations (30), we arrive at a set of linear partial derivative equations subject to the boundary conditions of the particular problem being traited.

6. Numerical solutions for piezoelectric bimorph in cylindrical bending

We consider a piezoelectric bimorph (see Fig. 2) undergoing a surface density of normal force and electric potential applied to the top and bottom faces of the plate. We assume that the shear traction is zero (i.e. $f_\alpha = 0$) and there is no surface density of moment ($\hat{m}_\alpha = 0$). The *simple support conditions* for a rectangular plate of length L are simulated by $\sigma_{11}(0,z) = \sigma_{11}(L,z) = 0$, $\sigma_{13}(0,z) = \sigma_{13}(L,z) = 0$ and $u_3(0,z) = u_3(L,z) = 0$. In this case the electromechanical variables do not depend on the y variable, accordingly the displacement u_2 plays any role in the problem and we set $U_2 = 0$ and $\gamma_2 = 0$.

The electromechanical load functions are written as Fourier series as follows:

$$(p(x), V(x)) = \sum_{n=1}^{\infty} (S_n, V_n) \sin(\lambda_n x), \tag{33}$$

with $\lambda_n = n\pi/L$, $S_n = 4S_0/n\pi$ and $V_n = 4V_0/n\pi$ if n odd and $S_n = V_n = 0$ if n even. Then, the loads thus defined represent uniform applied force density per unit of area S_0 and electric potential V_0. Sketches of the bimorph setting is given in Fig. 2 for both arrangements. A solution to the set of linear equations for the unknown functions which satisfies the boundary conditions for the cylindrical bending of a plate simply supported can be searched for as Fourier series

$$(U(x), \gamma(x)) = \sum_{n=1}^{\infty} (U_n, \Gamma_n) \cos(\lambda_n x), \tag{34}$$

$$\left(w(x), \phi_2^{(\ell)}(x), \phi_3(x)\right) = \sum_{n=1}^{\infty} \left(W_n, \Phi_{2,n}^{(\ell)}, \Phi_{3,n}\right) \sin(\lambda_n x), \tag{35}$$

and the same kind of series is considered for the Lagrangian multiplier

$$\theta(x) = \sum_{n=1}^{\infty} \Theta_n \sin(\lambda_n x). \tag{36}$$

The Fourier coefficients in Eqs. (34)–(36) are determined by substituting the solution into the equations of motion and solving simultaneously a set of linear algebraic equations for each n where the right-hand side contains the electromechanical loads given by Eq. (33). The set of linear algebraic equations can be put in matrix form

$$\mathbb{A}_n \mathbf{X}_n = \mathbf{B}_n, \tag{37}$$

where $\mathbb{A}_n$ is 7×7 matrix, the vector $\mathbf{X}_n = \{U_n, W_n, \Gamma_n, \Phi_{2,n}^{(1)}, \Phi_{2,n}^{(2)}, \Phi_{3,n}, \Theta_n\}$ contains the Fourier coefficients and the vector $\mathbf{B}_n$ defined the applied fields as functions of the Fourier factors S_n and V_n. The matrix $\mathbb{A}_n$ and vector $\mathbf{B}_n$ depend on λ_n, the thickness h and material constants of the bimorph. The detailed components of the matrix $\mathbb{A}_n$ and $\mathbf{B}_n$ are given in Appendix B. For the parallel bimorph, no Lagrange multiplier is considered and $\mathbb{A}$ is a matrix of 6×6 order (see Appendix B).

The geometry of the plate is $L = 25$ mm and $\ell = 12.5$ mm and different slenderness ratios are considered $L/h = 5$, 10 and 50. Two kinds of electromechanical loads are considered corresponding to (i) *sensor*

function with a force density per unit area applied to the upper face of the bimorph and (ii) *actuator function* with an electric potential applied to the top and bottom faces of the plate. However, the numerical results for state variables are given in dimensionless units as follows.

(i) for a surface density of force $S_0 \neq 0$ ($S_0 = 1000$ N/m^2, $V_0 = 0$) we set

$$(U, W, \Phi) = \frac{C_{11}^E}{hS_0}(u_1, u_3, \phi/E_0), \quad (T_{ij}, \mathscr{D}_k) = \frac{1}{S_0}(\sigma_{ij}, E_0 D_k), \tag{38}$$

(ii) for an applied electric potential $V_0 \neq 0$ ($V_0 = 50$ V and $S_0 = 0$) we set

$$(U, W, \Phi) = \frac{E_0}{V_0}(u_1, u_3, \phi/E_0), \quad (T_{ij}, \mathscr{D}_k) = \frac{hE_0}{C_{11}^E V_0}(\sigma_{ij}, E_0 D_k), \tag{39}$$

for numerical convenience we take $E_0 = 10^{10}$ V/m. The number of terms in the series Eqs. (33)–(36) are adjusted in order to satisfy the series convergence. The finite element computations for comparison are carried out with ABAQUS code by considering plane strain elements of 8-node biquadratic type and 800 elements are used. The results are also compared to those provided by a simplified model based on kinematic assumptions of Love–Kirchhoff's theory, it means that the shear correction is neglected. The bimorph is made of two identical layers of PZT-4 piezoelectric ceramics of which the material constants are given in Table 1 (extracted from Ikeda, 1996).

6.1. Series bimorph configuration

6.1.1. Sensor function

For this configuration the electric potential is set to zero and a surface density of normal force is applied to the top face of the bimorph. The numerical results are collected in Fig. 3 in dimensionless unit for the profiles with $L/h = 10$ and some estimating errors between the different approaches are given in Table 2 for three different aspect ratios. The elongation displacement U at $x = 0$ is plotted in Fig. 3(a), the profile is almost linear. The flexural displacement w at the middle of the plate ($x = L/2$) is given in Fig. 3(b), the straight line corresponds to the present plate approach. In Fig. 3(c) we have the induced electric potential showing an asymmetric profile. The shear stress σ_{13} computed at $x = L/4$ is depicted in Fig. 3(d). In this situation, it is clear that there is no global elongational motion of the plate, so that $U = 0$, as consequence $\phi_2^{(1)} + \phi_2^{(2)} = 0$ (see Eq. (13)). In addition the continuity condition for D_3 is then satisfied. This explains the asymmetric form of the electric potential profile. Comparisons to the finite element method and to the simplified model are presented in Table 2 for three typical slenderness ratios ($L/h = 5$, 10 and 50). The most interesting result is the discrepancy between the maximum values of the deflection at the plate center for the approaches. Indeed, the estimating errors for the deflection for the present model is about 0.007% for $L/h = 50$, 0.07% for $L/h = 10$ up to 2.5% for $L/h = 5$ (thick plate) while the error overtakes 13.8% for the simplified model. It is worthwhile noting the continuity of the shear stress σ_{13} through the interface between both piezoelectric layers while it is identically zero for the simplified model. The discrepancy for the maximum shear stress is 1.7% for $L/h = 50$, 2.9% for $L/h = 10$ and 5.67% for $L/h = 5$.

Table 1
Independent elastic, piezoelectric and dielectric constants of piezoelectric materials (transversally isotropic symmetry)

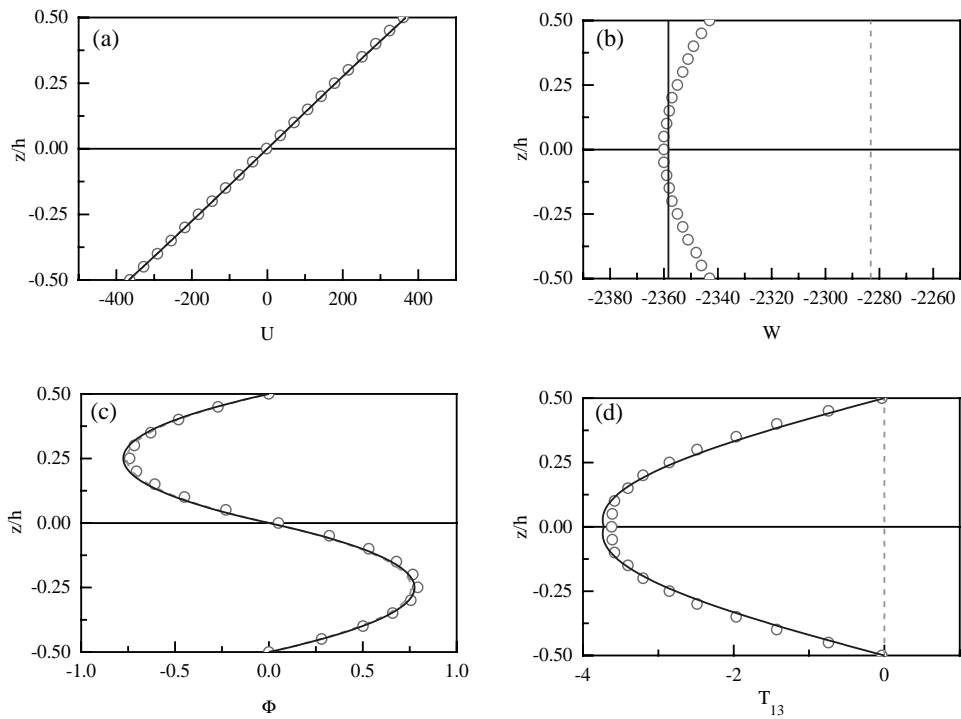|	C_{11}^E (GPa)	C_{12}^E	C_{33}^E	C_{13}^E	C_{44}^E	e_{31} (C/m^2)	e_{33}	e_{15}	ε_{11}^S (nF/m)	ε_{33}^S
PZT-4	139	77.8	115	74.3	25.6	−5.2	15.1	12.7	13.06	11.51

Fig. 3. Force density applied on the top face of a piezoelectric series bimorph in closed circuit for $L/h = 10$. Plate model (full line), finite element (small circles) and simplified plate model (dashed-line).
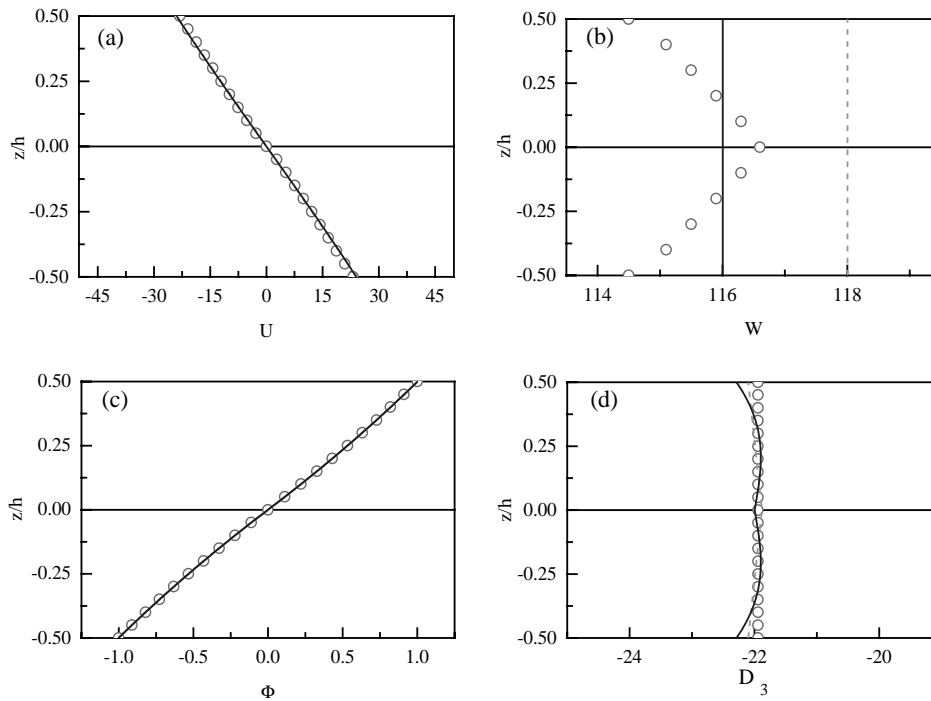
Table 2
Piezoelectric series bimorph, applied density force

L/h	Approaches	$W\ (L/2, 0)$	Error (%)	$\Phi\ (L/2, -h/4)$	Error (%)	$T_{13}\ (L/4, 0)$	Error (%)
50	FEM	-1.4286×10^6		19.0		-18.31	
	Present	-1.4287×10^6	0.007	18.986	0.007	-18.625	1.7
	LK	-1.4268×10^6	0.12	18.986	0.007	0.0	100.0
10	FEM	-2360.0		0.7925		-3.62	
	Present	-2358.36	0.07	0.775	2.15	-3.726	2.9
	LK	-2283.18	3.25	0.7574	4.43	0.0	100.0
5	FEM	-165.7		0.2234		-1.80	
	Present	-161.468	2.55	0.2063	7.64	-1.86	5.67
	LK	-142.74	13.85	0.188	15.7	0.0	100.0

6.1.2. Actuator function

In this situation, the piezoelectric bimorph suffers an electric potential applied to the top and bottom faces of the plate ($-V$ at $z = -h/2$ and $+V$ at $z = h/2$, with $p = 0$). The profile or local responses of the electromechanical variables are shown in Fig. 4. The longitudinal displacement u is plotted in Fig. 4(a), it displays very clearly a linear variation through the plate thickness with $u(z = 0) = 0$. This shows that the bimorph undergoes a bending motion. The deflection at the plate center and electric potential variations are presented in Fig. 4(b) and (c), respectively. An interesting result is the normal component of the electric induction $\mathscr{D}_3$ shown in Fig. 4(d) which is almost constant through the plate thickness. The errors in esti-

Fig. 4. Electric potential applied to a piezoelectric series bimorph for $L/h = 10$.

mating values between the present approach, the simplified model and finite element computation are given in Table 3 for three different aspects ratios. It should be noticed that the discrepancy of the deflection at the plate center does not exceed 2.3% for $L/h = 5$ (thick plate) in comparison to 4.8% for the simplified model (no shear correction). Moreover, for $L/h \geqslant 10$ the error is smaller than 0.5% which is excellent. With an applied electric potential of the order of 100 V, the bender produces a deflection of the order of 30 μm for $L/h = 50$. Table 3 also exhibits the errors in estimating the electric charge at the upper plate face and the jump of the longitudinal stress T_{11} at the interface for the three different slenderness ratios. The above results show the efficiency of the present refined approach to predict correctly both local state

Table 3
Electric potential applied to a piezoelectric series bimorph

L/h	Approaches	W $(L/2, 0)$	Error (%)	$[\![T_{11}]\!]$ $(L/2, 0)$	Error (%)	$\mathscr{D}_3$ $(L/2, h/2)$	Error (%)
50	FEM	2945.0		2.431		−21.94	
	Present	2943.3	0.02	2.422	0.36	−21.97	0.15
	LK	2945.3	0.05	2.413	0.74	−21.89	0.22
10	FEM	116.6		2.43		−21.94	
	Present	116.0	0.5	2.425	0.26	−21.995	0.25
	LK	118.0	1.2	2.412	0.78	−21.88	0.27
5	FEM	28.296		2.43		−21.94	
	Present	27.653	2.3	2.425	0.26	−21.99	0.25
	LK	29.651	4.8	2.412	0.78	−21.88	0.27

(through-the-thickness variation) and global responses for the sensor and actuator functions of the piezoelectric bimorph.

6.2. Parallel bimorph configuration

6.2.1. Sensor function

As in the case of the series arrangement, the electric potential is zero and a surface density of normal force is applied to the top face of the plate. The variation through the plate thickness for the deflection is given in Fig. 5(a) for the aspect ratio $L/h = 10$ at the plate center. The results of the present approach corresponds to the straight line while the simplified model is given by the dash-line and the small circle is for the finite element computation. The electric potential produced by the plate deformation through the piezoelectric coupling is shown in Fig. 5(b). The curve is symmetrical with respect to the plate mid-plane and it is piecewise parabolic curves. This demonstrates the usefulness of the quadratic part in the expansion of the electric potential (see Eq. (7) or (16)). The shear stress σ_{13} at $x = L/4$ is plotted in Fig. 5(c), in the present configuration the continuity condition of the shear stress is fulfilled. We notice the excellent agreement with the finite element result while it is almost zero for the simplified model. In Fig. 5(d), we have the normal component of the electric induction exhibiting a jump at the layer interface at the plate center. The jump in the electric induction provides the surface electric charge on the intermediate electrode. Table 4 gives some errors in estimating the global response of the bimorph structure for three different slenderness ratios ($L/h = 5$, 10 and 50). It is worthwhile noting that the error in estimating the deflection at the plate center is small (<1.5%) for the present model even for thick plates whereas it overtakes 10% for the simplified approach. The same remark holds for the induced electric potential. In the case of a bimorph structure with $L/h = 50$, the maximum electric potential induced within piezoelectric layers is about 0.7 V.
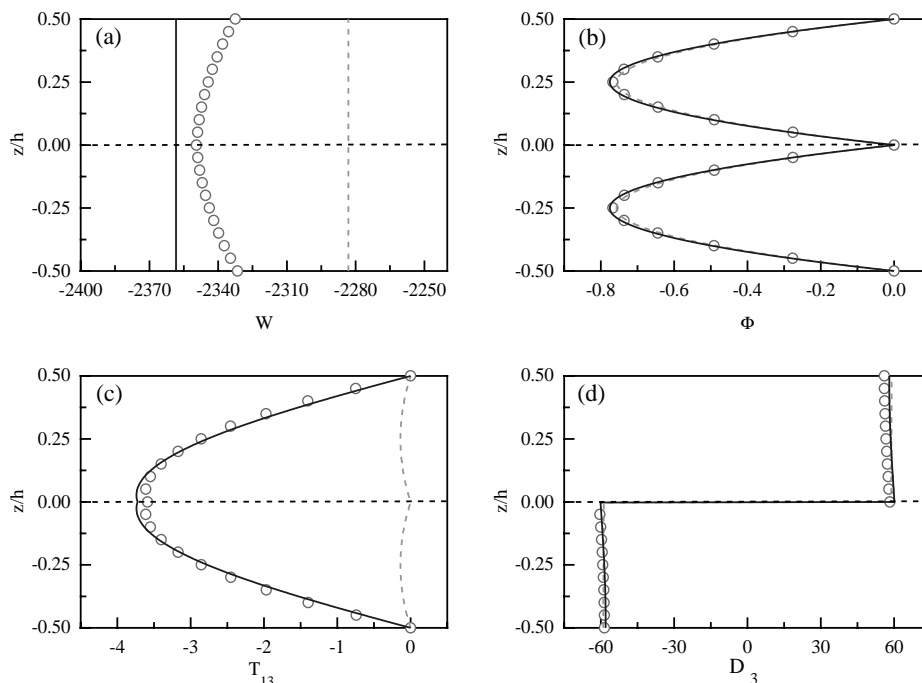

Fig. 5. Force density applied on the top face of a piezoelectric parallel bimorph in closed circuit for $L/h = 10$.

Table 4
Piezoelectric parallel bimorph, applied density force

L/h	Approaches	W $(L/2, 0)$	Error (%)	Φ $(L/2, -h/4)$	Error (%)	T_{13} $(L/4, 0)$	Error (%)
50	FEM	-1.4285×10^6		-18.977		-17.94	
	Present	-1.4287×10^6	0.016	-18.986	0.047	-18.62	3.8
	LK	-1.4268×10^6	0.116	-18.968	0.049	0.0	100.0
10	FEM	-2349.4		-0.766		-3.587	
	Present	-2358.4	0.38	-0.775	1.15	-3.724	3.8
	LK	-2283.2	2.82	-0.757	1.21	0.0	100.0
5	FEM	-159.21		-0.197		-1.793	
	Present	-161.47	1.4	-0.206	4.45	-1.861	3.8
	LK	-142.74	10.3	-0.188	23.7	0.0	100.0

In addition, the electric charge produced at the layer interface is $Q_{\text{tot}} = [\![\mathscr{D}_3]\!]_{z=0} \times L \times \ell$ and it is of the order of 1 C ($L \times \ell$ is the surface of the intermediate metallic electrode).

6.2.2. Actuator function

In this situation the piezoelectric bimorph is subject to an electric potential applied to the bottom and top faces of the plate (V at $z = \pm h/2$) and the intermediate electrode is set to zero voltage. The through-the-thickness variation of the electromechanical quantities are collected together in Fig. 6 for $L/h = 10$. The
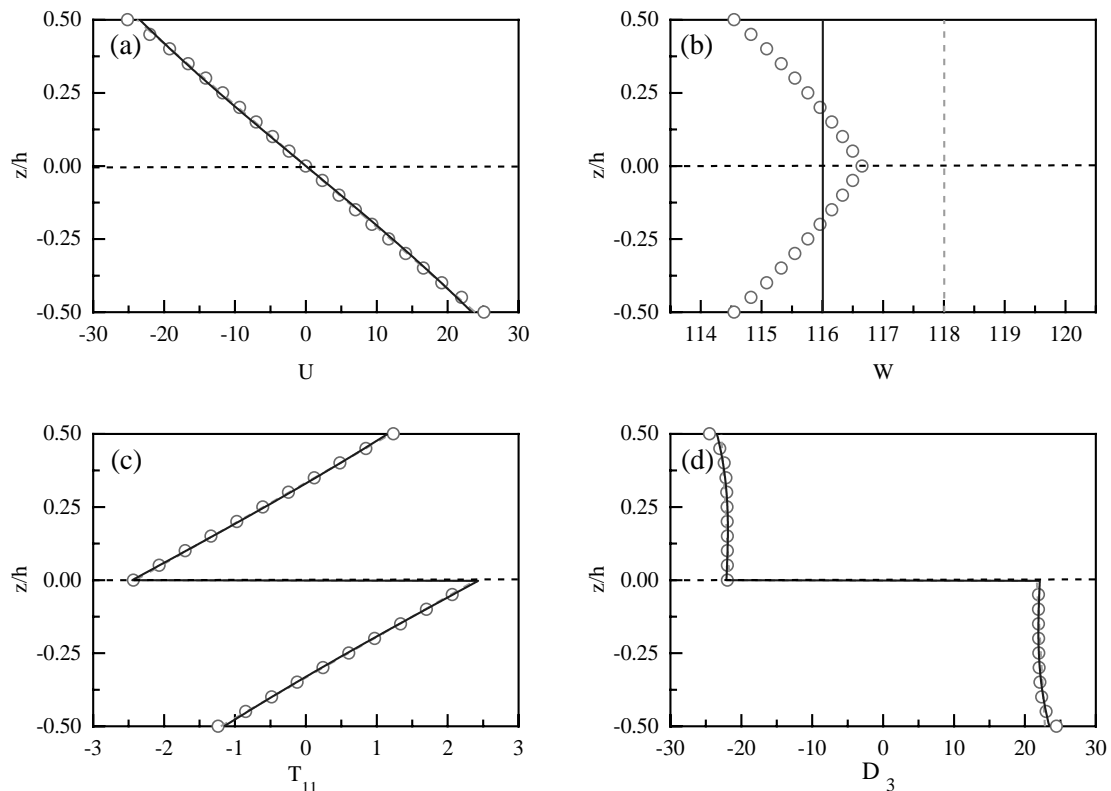

Fig. 6. Electric potential applied to a piezoelectric parallel bimorph for $L/h = 10$.

Table 5
Electric potential applied to a piezoelectric parallel bimorph

L/h	Approaches	W $(L/2,0)$	Error (%)	$[\![T_{11}]\!]$ $(L/2,0)$	Error (%)	$[\![\mathscr{D}_3]\!]$ $(L/2,0)$	Error (%)
50	FEM	2943.9		4.89926		44.222	
	Present	2943.3	0.02	4.89817	0.02	44.213	0.02
	LK	2945.3	0.05	4.89645	0.06	44.198	0.054
10	FEM	115.5		4.8614		43.88	
	Present	116.0	1.27	4.8974	0.74	44.195	0.72
	LK	118.0	3.0	4.8007	1.25	43.343	1.22
5	FEM	26.197		4.8413		43.879	
	Present	27.654	5.56	4.9251	1.31	44.436	1.27
	LK	29.651	13.2	4.7853	1.56	43.205	1.53

longitudinal or axial displacement is given in Fig. 6(a), it has almost linear variation. The resulting deflection at the plate center is shown in Fig. 6(b). The full straight line corresponds to the present model while the dash-line curve is for the simplified model (no shear correction). It is noticed that the deflection for the present model is closer to the finite element result than the simplified model is. In Fig. 6(c), we have the axial stress with a discontinuity at the layer interface. Nevertheless, the most interesting result is the profile of the normal component of the electric induction D_3 depicted in Fig. 6(d). It is observed that the electric induction undergoes a jump at the bimorph interface, this means that a surface density of electric charge is then produced on the intermediate electrode given by $[\![D_3]\!]_{z=0} = Q$. Some estimates are given in Table 5 for three slenderness ratios ($L/h = 5$, 10 and 50) and comparisons with finite element computation and simplified model are also considered. Table 5 tells us that the present model provides quite good results, especially the discrepancy in the deflection at the plate center is less than 6%, for the jump of the axial stress and that of the electric induction at the layer interface, it is less than 1.5%. Going back to the physical dimensions, a deflection of about 30 μm is obtained when a voltage of 100 V is applied for $L/h = 50$. The deflection thus produced is of the same order than that of the series arrangement (see Section 6.1.2). The jump of the axial stress at $z = 0$ is of the order of 13.6 MPa. The electric charge measured on the intermediate metallic electrode at $z = 0$ is about 40 C.

7. Vibration of piezoelectric bimorph

In this section, we consider dynamical processes for the piezoelectric bimorph based on the present modelling. Then we propose the prediction of modal frequencies of the structure for both open circuit ($D_3 = 0$) and closed circuit ($\phi = 0$) conditions on the top and bottom faces of the bimorph, for the typical aspect ratio $L/h = 10$. The knowledge of modal frequencies of such piezoelectric elements plays an increasingly important role in the *control process of vibrations* as suggested by Anderson and Hagood (1990). In particular, piezoelectric composites can be used as components of a passive damping device, thereby avoiding complex control and feedback systems. Piezoelectric composites have the ability to convert kinetic energy to electric energy during vibration process and vice versa. This enables the dissipation of electric energy through a passive electric circuitry (i.e., shunt resistor). Works have been reported on passive control of vibration through piezoelectric elements have been reported by Gaudenzi et al. (2000) and Vidoli and Dell'Isola (2001). The sensitivity of the performance of such a passive control of vibrations to the optimal tuning of the resonant electric circuitry is only obtained by an accurate prediction of the modal frequencies. At this end, piezoelectric bimorph structures turn out to be an interesting element for vibration control.

The solution to the piezoelectric plate equations (30) depends on time by introducing the factor $e^{i\omega t}$ in the Fourier series equations (33)–(36). Now, the Fourier coefficients of the solution are searched for by solving an homogeneous set of linear equations taking on the form

$$\mathbb{A}_n(\Omega)\mathbf{X}_n = \mathbf{0}, \tag{40}$$

instead of Eq. (37) in the static case. The subscript n represents the mode number. The matrix $\mathbb{A}_n$ depends on the normalized circular frequency $\Omega = \sqrt{\rho/C_{11}^*}h\omega$. Non-zero solution to Eq. (40) yields

$$\det(\mathbb{A}_n(\Omega)) = 0, \tag{41}$$

giving rise to eigenmodes of the bimorph structure for a given n. The right-hand side of Eq. (37) is zero, since only free vibrations are considered. The conditions are those of the cylindrical bending. In the case of the series configuration, the matrix $\mathbb{A}_n$ is 7×7 order for the closed circuit condition whereas it is 10×10 order for the open-circuit setting. For the parallel arrangement, there is no Lagrange multiplier, the matrix $\mathbb{A}_n$ is 6×6 order for the closed-circuit condition and it is 9×9 order for the open-circuit case.

The frequencies of the resonant modes are presented in Tables 6 and 7 in comparison to the results provided by finite element computations first and to the estimates given by the simplified version of the model next. The results are given for the aspect ratios $L/h = 10$. However additional results can be found in Fernandes (2000) for different slenderness ratios ($L/h = 5$ and 50). The numerical results show that the piezoelectric bimorph has a series of natural bending and axial modes. Table 6 gives the first seven bending vibration frequencies and the first axial frequency for the closed circuit condition. It is clear there is tiny difference between the present model and the simplified one for the axial mode since the shear correction does not play any role in this mode. Nevertheless, a rather good agreement is observed for the refined model

Table 6
Modal frequencies for the piezoelectric bimorph in closed circuit ($L/h = 10$)

Frequencies (Hz)—$L/h = 10$					
Modes	EF	Present model	Error (%)	Simplified model	Error (%)
Flex. $n = 1$	15,747	15,769	0.1	16,030	1.8
Flex. $n = 2$	59,370	59,677	0.5	63,338	6.3
Flex. $n = 3$	122,994	124,291	1	139,721	12
Flex. $n = 4$	199,046	202,511	1.7	241,909	17.7
Flex. $n = 5$	282,019	289,352	2.5	366,039	22.9
Flex. $n = 6$	368,241	381,771	3.5	508,113	27.5
Flex. $n = 7$	455,253	478,014	4.8	664,352	31.5
Axial $n = 1$	188,372	188,599	0.1	188,599	0.1

Table 7
Modal frequencies for the piezoelectric bimorph in open circuit ($L/h = 10$)

Frequencies (Hz)—$L/h = 10$					
Modes	EF	Present model	Error (%)	Simplified model	Error (%)
Flex. $n = 1$	16,656	16,681	0.1	17,034	2.2
Flex. $n = 2$	62,024	62,375	0.5	67,200	7.7
Flex. $n = 3$	126,722	128,194	1	147,886	14.3
Flex. $n = 4$	202,683	206,520	1.7	255,305	20.6
Flex. $n = 5$	282,019	284,741	2.5	385,109	26.1
Flex. $n = 6$	369,814	384,032	3.5	532,926	30.6
Flex. $n = 7$	455,974	479,291	4.8	694,727	34.4
Axial $n = 1$	188,478	188,618	0.1	188,599	0.06

even for higher modes. On the other hand the simplified model based on the kinematic assumption of Love–Kirchhoff elastic plate theory provides very non accurate values for the frequencies of the bending modes. This demonstrates the beneficial role played by the shear function and the layerwise approximation for the electric potential in the prediction of the frequencies of bending modes. The results and comparisons for the slenderness ratio $L/h = 10$ are collected in Table 7 for the open circuit condition. Here, once again, the present model is definitly better than the simplified model for the first seven bending modes. The effectiveness of the present accurate modelling pleads in its favour for the use of piezoelectric bimorph in actively or passively controlling vibrations of elastic structures.

8. Concluding remarks

In the present study the piezoelectric bimorph structure has been investigated in details for its actuator and sensor functions statically and dynamically (vibration). It is clear that in the light of the numerical simulations and comparisons, the model has excellent performances. The approach is mainly based on the principle of linear piezoelectricity in the framework of the quasi-electrostatic hypothesis. The model thus presented is based on the combination of an equivalent single-layer approach for the mechanical displacements with a layerwise type of modelling for the electric potential considered as an additional degree of freedom. Two types of arrangement have been investigated, series and parallel bimorphs. For the latter an intermediate metallic electrode at the layer interface allows one to accommodate an applied electric potential. Moreover, the present approach includes the correction of the shear effect, which has a key role in the accuracy of the results. The numerical simulations and comparisons assess of the quality of the prediction of global and local responses (the through-the-thickness variation of the mechanical and electric variables) for static and dynamic processes. Especially, the approach to piezoelectric bimorph provides very accurate prediction of the bending and elongational vibration frequencies even for rather thick plate ($L/h = 5$), whereas classical elastic thin plate theory based on Love–Kirchhoff theory gives less accurate results with increasing discrepancy (more than 30% for $L/h = 5$). Smits et al. (1991a), Smits and Cooney (1991b) have reported interesting results on the global responses of piezoelectric bimorph (maximum of deflection, induced electric charges, etc.) based on Bernoulli–Euler beam theory. On using asymptotic approach He et al. (2000) and Lim et al. (2001) have derived the equations of motion for piezoelectric (parallel and antiparallel) bimorphs and they have obtained similar results for the through-the-thickness variation of electromechanical fields.

The results here above obtained for piezoelectric bimorph will be completed by the investigations of other configurations, for instance, the piezoelectric bimorph with one layer considered as sensor function and the other layer used as actuator function seems to be an interesting practical problem. Constituent equations for the bimorph describing the relationship between the electromechanical resultants (force, moment, voltage) applied to the bimorph and global responses of the structure (deflection, rotation, electric charge or current) is useful for engineering devices (e.g., micro-positionner, etc.). These problems will be tackled in future works.

Appendix A. Effective material constants

All the algebraic manipulations have been done under the normal shear stress hypothesis for elastic thin plates (σ_{33} negligible in comparison to the other stress components). This leads to define effective modulus of elasticity (using Voigt notation)

$$C_{ab}^* = C_{ab}^E - \frac{C_{a3}^E C_{3b}^E}{C_{33}^E}, \tag{A.1}$$

effective piezoelectric coefficients

$$e_{ja}^* = e_{ja} - \frac{e_{j3}C_{a3}^{\mathrm{E}}}{C_{33}^{\mathrm{E}}}, \tag{A.2}$$

effective dielectric constants

$$\epsilon_{ij}^* = \epsilon_{ij}^{\mathrm{S}} + \frac{e_{i3}e_{j3}}{C_{33}^{\mathrm{E}}}, \tag{A.3}$$

respectively, with $a, b \in \{1, \ldots, 6\}$, $i, j \in \{1, 2, 3\}$.

Appendix B. Matrix $\mathbb{A}_n$ for series and parallel bimorphs

The matrix and the right-hand side of the set of linear algebraic equations given in Eq. (37) takes on the following form.

(a) *For the series configuration*

$$\mathbb{A}_n = \begin{bmatrix} a_{11} & 0 & 0 & 0 & 0 & a_{16} & a_{17} \\ & a_{22} & a_{23} & a_{24} & a_{25} & 0 & 0 \\ & & a_{33} & a_{34} & a_{35} & 0 & 0 \\ & \text{(sym.)} & & a_{44} & 0 & a_{46} & a_{47} \\ & & & & a_{55} & a_{56} & a_{57} \\ & & & & & a_{66} & 0 \\ & & & & & & 0 \end{bmatrix}, \tag{B.1}$$

where the matrix components are defined by

$$a_{11} = -\Lambda_n^2 C_{11}^{*\prime}, \quad a_{33} = -\frac{1}{2}\left[\left(\frac{\Lambda_n}{\pi}\right)^2 C_{11}^{*\prime} + C_{55}^{*\prime}\right],$$

$$a_{16} = -2\left(\frac{\Lambda_n}{\pi}\right)e_{31}^{*\prime}, \quad a_{34} = -a_{35} = \frac{2}{\pi^2}\left(\frac{\Lambda_n}{\pi}\right)\left(\frac{\pi}{4} - 1\right)\left(e_{31}^{*\prime} + e_{15}^{*\prime}\right),$$

$$a_{17} = -2\Lambda_n e_{31}^{*\prime}, \quad a_{44} = a_{55} = \frac{1}{24}\left[\frac{1}{10}\left(\frac{\Lambda_n}{2}\right)^2 \varepsilon_{11}^{*\prime} + \varepsilon_{33}^{*\prime}\right],$$

$$a_{22} = -\frac{1}{12}\Lambda_n^4 C_{11}^{*\prime}, \quad a_{46} = a_{56} = \frac{2}{\pi^2}\left(\frac{\pi}{4} - 1\right)\left[\left(\frac{\Lambda_n}{\pi}\right)^2 \varepsilon_{11}^{*\prime} + \varepsilon_{33}^{*\prime}\right],$$

$$a_{23} = 2\left(\frac{\Lambda_n}{\pi}\right)^3 C_{11}^{*\prime}, \quad a_{47} = a_{57} = -\frac{1}{2}\varepsilon_{33}^{*\prime},$$

$$a_{24} = -a_{25} = \frac{1}{12}\left(\frac{\Lambda_n}{2}\right)^2 e_{31}^{*\prime}, \quad a_{66} = \frac{1}{2}\left[\left(\frac{\Lambda_n}{\pi}\right)^2 \varepsilon_{11}^{*\prime} + \varepsilon_{33}^{*\prime}\right],$$

and the vector $\mathbf{B}_n$ is defined by

$$\mathbf{B}_n = \begin{bmatrix} 0, & b_2, & b_3, & b_4, & b_5, & b_6, & 0 \end{bmatrix}^{\mathrm{T}}, \tag{B.2}$$

with the components given by

$$b_2 = \widehat{S}_n + \frac{1}{2} \Lambda_n^2 e_{31}^{*\prime} \widehat{V}_n,$$

$$b_3 = -\frac{4}{\pi} \left(\frac{\Lambda_n}{\pi} \right) e_{31}^{*\prime} \widehat{V}_n,$$

$$b_4 = b_5 = -\frac{1}{6} \left(\frac{\Lambda_n}{4} \right)^2 \varepsilon_{11}^{*\prime} \widehat{V}_n,$$

$$b_6 = \left(\frac{4}{\pi} \right) \varepsilon_{33}^{*\prime} \widehat{V}_n.$$

(b) *For the parallel configuration*

$$\mathbb{A}_n = \begin{bmatrix} a_{11} & 0 & 0 & 0 & 0 & 0 \\ & a_{22} & a_{23} & a_{24} & a_{25} & a_{26} \\ & & a_{33} & a_{34} & a_{35} & a_{36} \\ & \text{(sym.)} & & a_{44} & 0 & a_{46} \\ & & & & a_{55} & a_{56} \\ & & & & & a_{66} \end{bmatrix}, \tag{B.3}$$

where the components of the matrix $\mathbb{A}_n$ are defined by

$$a_{11} = -\Lambda_n^2 C_{11}^{*\prime},$$

$$a_{22} = -\frac{1}{12} \Lambda_n^4 C_{11}^{*\prime},$$

$$a_{23} = 2 \left(\frac{\Lambda_n}{\pi} \right)^3 C_{11}^{*\prime},$$

$$a_{24} = a_{25} = -\frac{1}{12} \left(\frac{\Lambda_n}{2} \right)^2 e_{31}^{*\prime},$$

$$a_{26} = -2 \left(\frac{\Lambda_n}{\pi} \right)^2 \left(\frac{\pi}{4} - 1 \right) e_{31}^{*\prime},$$

$$a_{33} = -\frac{1}{2} \left[\left(\frac{\Lambda_n}{\pi} \right)^2 C_{11}^{*\prime} + C_{55}^{*\prime} \right],$$

$$a_{34} = a_{35} = -\frac{2}{\pi^2} \left(\frac{\Lambda_n}{\pi} \right) \left(\frac{\pi}{4} - 1 \right) \left(e_{31}^{*\prime} + e_{15}^{*\prime} \right),$$

$$a_{36} = \frac{4}{\pi^2} \left(\frac{\Lambda_n}{\pi} \right) \left(\frac{\pi^2}{8} - 1 \right) \left(e_{31}^{*\prime} + e_{15}^{*\prime} \right),$$

$$a_{44} = a_{55} = \frac{1}{24} \left[\frac{1}{10} \left(\frac{\Lambda_n}{2} \right)^2 \varepsilon_{11}^{*\prime} + \varepsilon_{33}^{*\prime} \right],$$

$$a_{46} = a_{56} = \frac{2}{\pi^2} \left[\left(\frac{\Lambda_n}{\pi} \right)^2 \left(\frac{1}{3} \left(\frac{\pi}{4} \right)^3 + \frac{\pi}{4} - 1 \right) \varepsilon_{11}^{*\prime} + \left(\frac{\pi}{4} - 1 \right) \varepsilon_{33}^{*\prime} \right],$$

$$a_{66} = \left(\frac{2}{\pi} \right)^2 \left[\left(\frac{\pi^2}{8} - 1 \right) \varepsilon_{33}^{*\prime} + 2 \left(\frac{\Lambda_n}{\pi} \right)^2 \left(\frac{5}{48} \pi^2 - 1 \right) \varepsilon_{11}^{*\prime} \right],$$

and the vector $\mathbf{B}_n$ is defined as follows:

$$\mathbf{B}_n = \begin{bmatrix} 0, & b_2, & b_3, & b_4, & b_5, & b_6 \end{bmatrix}^{\mathrm{T}}, \tag{B.4}$$

with the components given by

$$b_2 = \widehat{S}_n + \frac{1}{2}\Lambda_n^2 e_{31}^{*\prime}\widehat{V}_n,$$

$$b_3 = \Lambda_n\left(\frac{2}{\pi}\right)^2\left[\left(\frac{\pi}{2}-1\right)e_{15}^{*\prime} - e_{31}^{*\prime}\right]\widehat{V}_n,$$

$$b_4 = b_5 = \frac{1}{6}\left(\frac{\Lambda_n}{4}\right)^2 \varepsilon_{11}^{*\prime}\widehat{V}_n,$$

$$b_6 = \frac{4}{\pi}\left(\frac{\Lambda_n}{\pi}\right)^2\left(\frac{1}{6}\left(\frac{\pi}{2}\right)^2 - \frac{\pi}{2} + 1\right)\varepsilon_{11}^{*\prime}\widehat{V}_n.$$

In the above definition we have set $\Lambda_n = h\lambda_n = n\pi(h/L)$ placing the inverse of the slenderness ratio $\frac{L}{h}$ in evidence. It is worthwhile noting that some components of the matrices (B.1) and (B.3) are the same or opposite. In addition, we have introduced the dimensionless electromechanical variables and material constants defined as follows

$$\left(\widehat{U}_n, \widehat{W}_n, \widehat{\Gamma}_n, \widehat{\Phi}_{2,n}^{(\ell)}, \widehat{\Phi}_{3,n}, \widehat{\Theta}_n, \widehat{S}_n, \widehat{V}_n\right) = \left(\frac{U_n}{h}, \frac{W_n}{h}, \Gamma_n, \frac{h\Phi_{2,n}^{(\ell)}}{E_0}, \frac{\Phi_{3,n}}{E_0}, \frac{\theta_n}{h}, \frac{S_n}{C_{00}}, \frac{V_n}{hE_0}\right),$$

$$\left(C_{\alpha\beta}^{*\prime}, e_{i\alpha}^{*\prime}, \varepsilon_{ij}^{*\prime}\right) = \left(\frac{C_{\alpha\beta}^*}{C_{00}}, \frac{E_0 e_{i\alpha}^*}{C_{00}}, \frac{E_0^2 \varepsilon_{ij}^*}{C_{00}}\right),$$

where the constant C_{00} is an elastic modulus of reference, for numerical investigations we take C_{11} and E_0 has been given in Section 6.

References

Anderson, E.H., Hagood, N.W., 1990. Simultaneous piezoelectric sensing/actuator: analysis and application to controlled structures. J. Sound Vibr. 174, 617–639.

Bisegna, P., Caruso, G., 2001. Evaluation of higher-order theories of piezoelectric plates in bending and in stretching. Int. J. Solids Struct. 38, 8805–8830.

Cady, W.G., 1964. Piezoelectricity. Dover, New York.

Chee, C.Y.K., Tong, L., Steven, G.P., 1998. A review on the modeling of piezoelectric sensors and actuators incorporated in intelligent structures. J. Intell. Mater: Syst. Struct. 9, 3–19.

Chonan, S., Jiang, Z.W., Koseki, M., 1996. Soft-handling gripper driven by piezoceramic bimorph strips. Smart Mater. Struct. 5, 407–414.

Crawley, E.F., Anderson, E.H., 1990. Detailed model of piezoceramic actuation of beam. J. Intell. Mater: Syst. Struct. 1, 4–25.

Fernandes, A., 2000. Modèle et étude de composants piézoélectriques: applications aux structures mulifonctionnelles. Ph.D. Thesis at University Paris VI.

Fernandes, A., Pouget, J., 2001. Accurate modelling of piezoelectric plates: single-layered plate. Arch. Appl. Mech. 71, 509–524.

Fernandes, A., Pouget, J., 2002. An accurate modelling of piezoelectric multi-layer plates. Eur. J. Mech. A/Solids 21, 629–651.

Gaudenzi, P., Carbonaro, R., Benzi, E., 2000. Control of beam vibrations by means of piezoelectric devices: theory and experiments. Compos. Struct. 50, 373–379.

He, L.-H., Lim, C.W., Soh, A.K., 2000. Three-dimensional analysis of an antiparallel piezoelectric bimorph. Acta Mech. 145, 189–204.

Ikeda, T., 1996. Fundamental of Piezoelectricity. Oxford University Press, Oxford.

Lee, J.K., 1979. Piezoelectric bimorph optical beam scanners: analysis and construction. Appl. Opt. 18, 454–459.

Lim, C.W., He, L.-H., Soh, A.K., 2001. Three-dimensional electromechanical responses of a parallel piezoelectric bimorph. Int. J. Solids Struct. 38, 2833–2849.

Love, A.E.H., 1944. Treatise on the Mathematical Theory of Elasticity. Dover, New York.

Muralt, P., Pohl, D.W., Denk, W., 1986. Wide-range, low-operating-voltage, bimorph STM: application as potentiometer. IBM J. Res. Develop. 30, 443–450.

Peters, D.J., Blackford, B.L., 1989. Piezoelectric bimorph-based translation device for two-dimensional, remote micropositioning. Rev. Sci. Instrum. 80, 138–140.

Rao, S.S., Sunar, M., 1994. Piezoelectricity and its use in disturbance sensing and control of flexible structures: a survey. Appl. Mech. Rev. 47, 113–123.

Reddy, J.N., 1984. A simple higher-order theory for laminated composite plates. J. Appl. Mech., 745–752.

Reissner, E., 1975. On the transverse bending of plates including the effect of transverse shear deformation. Int. J. Solids Struct. 11, 569–573.

Saravanos, D.A., Heyliger, P.R., 1999. Mechanics and computational models for laminated piezoelectric beams, plates and shells. Appl. Mech. Rev. 52, 305–320.

Smits, J.G., Dalke, S.I., Cooney, T.K., 1991a. The constituent equations of piezoelectric bimorphs. Sensors Actuat. A—Physics A 28, 41–61.

Smits, J.G., Cooney, T.K., 1991b. The effectiveness of a piezoelectric bimorph actuator to perform mechanical work under various constant loading conditions. Ferroelectrics 119, 89–105.

Spineau, A., Billet, D., Kielbasa, R., 1998. A piezoelectric cantilever bimorph with both sensor and summer functions: theoretical study of its quasistatic response. In: Mechanical Transducers Proceedings of Eurosensors XII. I.U.P. Publishing Ltd., pp. 419–422.

Steel, M.R., Harrison, F., Harper, P.G., 1978. The piezoelectric bimorph: an experimental and theoretical study of its quasistatic response. J. Phys. D: Appl. Phys. 11, 979–989.

Tani, J., Takagi, T., Qiu, J., 1998. Intelligent material systems: application of functional materials. Appl. Mech. Rev. 51, 5005–5021.

Tiersten, H.F., 1969. Linear Piezoelectric Plate Vibrations. Plenum Press, New York.

Touratier, M., 1991. An efficient standard plate theory. Int. J. Eng. Sci. 29, 901–916.

Touratier, M., 1992. A refined theory of laminated shallow shells. Int. J. Solids Struct. 29, 1401–1415.

Vidoli, S., Dell'Isola, F., 2001. Vibration control in plates by uniformly distributed actuators interconnected via electric networks. Eur. J. Mech. A/Solids 20, 435–456.

Yoon, J.S., Washington, G., 1998. Piezoceramic actuated aperture antennae. Smart Mater. Struct. 7, 537–542.